ACS APPLIED MATERIALS & INTERFACES

Research Article

www.acsami.org

Modulation of Bone-Specific Tissue Regeneration by Incorporating Bone Morphogenetic Protein and Controlling the Shell Thickness of Silk Fibroin/Chitosan/Nanohydroxyapatite Core–Shell Nanofibrous Membranes

K. T. Shalumon,[†,‡] Guo-Jyun Lai,[†,‡] Chih-Hao Chen,[†,§] and Jyh-Ping Chen*[,†]

[†]Department of Chemical and Materials Engineering, Chang Gung University, Kwei-San, Taoyuan 333, Taiwan Republic of China

[§]Department of Plastic and Reconstructive Surgery, Chang Gung Memorial Hospital, Chang Gung University, College of Medicine, Kwei-San, Taoyuan 333, Taiwan Republic of China

Supporting Information

ABSTRACT: The presence of both osteoconductive and osteoinductive factors is important in promoting stem cell differentiation toward the osteogenic lineage. In this study, we prepared silk fibroin/chitosan/nanohydroxyapatite/bone morphogenetic protein-2 (SF/CS/nHAP/BMP-2, SCHB2) nanofibrous membranes (NFMs) by incorporating BMP-2 in the core and SF/CS/nHAP as the shell layer of a nanofiber with two different shell thicknesses (SCHB2-thick and SCHB-thin). The physicochemical properties of SCHB2 membranes were characterized and compared with those of SF/CS and SF/CS/nHAP NFMs. When tested in release studies, the release rate of BMP-2 and the concentration of BMP-2 in the release medium were higher for SCHB2-thin NFMs because of reduced shell thickness. The BMP-2 released from the nanofiber retained its osteoinductive activity toward human-bone-marrow-derived mesenchymal stem cells (hMSCs). Compared with SF/CS and SF/CS/nHAP NFMs, the incorporation of BMP-2-promoted osteogenic differentiation of hMSCs and the SCHB-thin NFM is the best scaffold during in vitro cell culture. Gene expression analysis by real-time quantitative polymerase chain reaction detected the evolution of both early and late marker genes of bone formation. The relative mRNA expression is in accordance with the effect of BMP-2 incorporation and shell thickness, while the same was reconfirmed through the quantification of bone marker protein osteocalcin. In vivo experiments were carried out by subcutaneously implanting hMSC-seeded SCHB2-thin NFMs and acellular controls on the back sides of nude mice. Immunohistochemical and histological staining confirmed ectopic bone formation and osteogenesis of hMSCs in SCHB2-thin NFMs. In conclusion, the SCHB2-thin NFM could be suggested as a promising scaffold for bone tissue engineering.

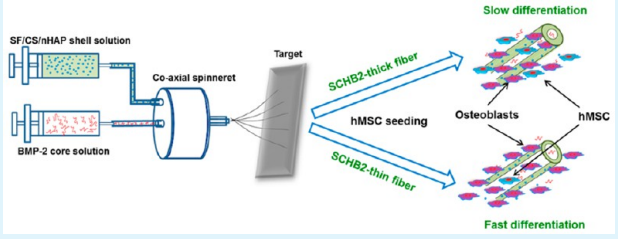

KEYWORDS: *silk fibroin, chitosan, bone morphogenetic protein, core–shell nanofibers, bone tissue engineering, coaxial electrospinning*

1. INTRODUCTION

Tissue engineering necessitates biomaterials having extracellular matrix (ECM) mimicking environments with controllable material properties.[1] Considering human bone, it consists of a large amount of hydroxyapatite (HAP) and collagen, along with small amounts of polysaccharides, proteins, and lipids.[2,3] In addition, the clinical needs for bone regeneration aroused from bone defects occurs through resection of primary and metastatic tumors, skeletal trauma bone loss, trabecular voids, etc. The current clinical scenario is mainly inclined on the autograft–allograft as well as nonbiodegradable polymeric implant methods.[4] However, the limited supply of autograft bones, risk of disease transfer of allografts,[5] high polymerization temperature of nonbiodegradable implants, and leachable toxic small molecules[6,7] necessitates the development of an ideal scaffold that could mimic all of the functionalities of a natural ECM by supporting cell attachment, proliferation, and differentiation. Also, scaffolds with osteoinducing factors[8] and nano/microscale surface topography could accelerate the regeneration rate by favorably enhancing the cell binding sites.[9]

Degradation of biodegradable materials is crucial in bone regeneration because it directly influences the mechanical integrity of a scaffold. Moreover, scaffolds with toxic degradation byproducts might alter the tissue microenvironment and thus challenge the biocompatibility of the material.[10] Systematic administration of conductive/inductive factors in scaffolds with controlled release/degradation potentials and macroporosity could provide a suitable environment for ECM production.[11,12] One of the most common and widely accepted scaffold architectures for bone tissue engineering is composite polymeric materials, in which nanohydroxyapatite (nHAP) would be an osteoconductive component. Such scaffolds can

Received: June 5, 2015
Accepted: September 10, 2015
Published: September 10, 2015

DOI: 10.1021/acsami.5b04962
ACS Appl. Mater. Interfaces 2015, 7, 21170–21181

Scheme 1. Schematic Representation of the Preparation of SCHB2-Thick and SCHB2-Thin NFMs through Coaxial Electrospinning and Their Influence on hMSCs

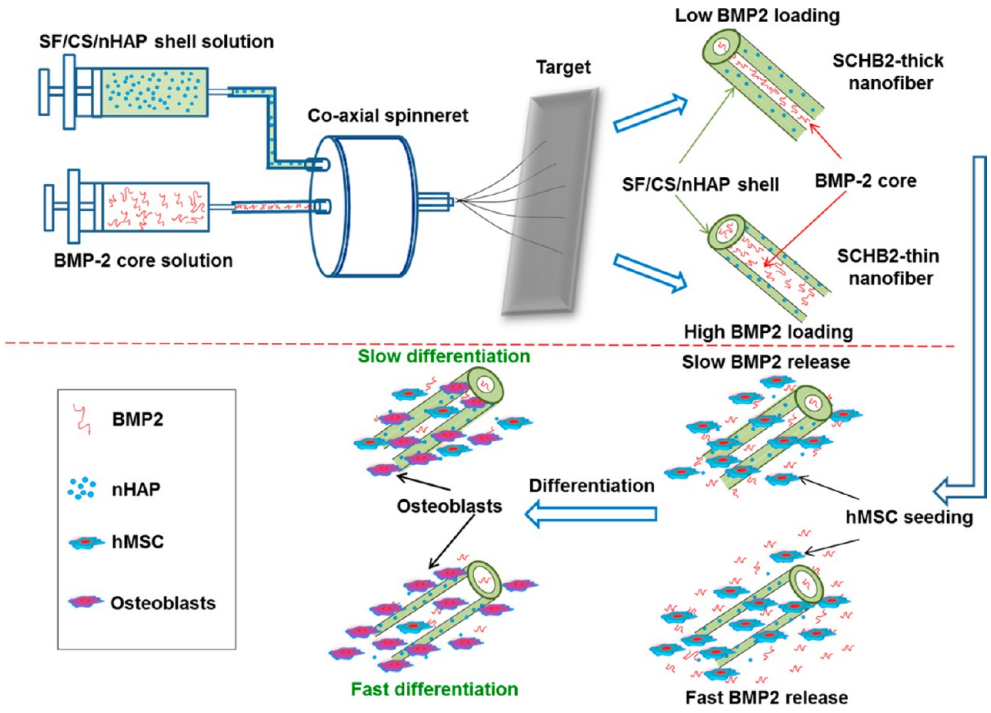

induce the preosteoblasts to an osteogenic phenotype through appropriate cell−material interactions. Numerous methods are currently available for producing scaffold architecture with both micro/nano- and macroenvironments. By adjustment of the biomechanical properties through structural arrangement and chemical constituents, the functionality of the scaffold and its degradation byproducts can be controlled.[13] However, conventional techniques, like gas foaming,[14] freeze-drying,[15] salt leaching,[16] blending,[17] etc., are not efficient enough to create nanoscale morphologies to simulate bone ECM.[18] Moreover, a better design capable of combining nanofibers/nanoparticles with osteoconductive/inductive factors is essential. This could be achieved through electrospinning, a well-known technique for producing fibers in the range of a few nanometers to several micrometers.[19]

Although various polymeric materials are currently used for producing electrospun nanofibers, natural polymers are of great importance because of their natural origin and nontoxicity of degradation products. The vast availability, reproducibility, and minimum risk of disease transfer made them suitable for various tissue repair applications.[20,21] The rate of regeneration is much influenced by the presence of inducing factors such as osteoconductive ceramic particles or osteoinductive growth factors. Our previous reports already confirmed the osteoconductive properties of chitosan (CS) when used along with silk fibroin (SF).[21] Being natural in origin and having structural similarity to glycoaminoglycans, CS is useful in the differentiation of bone marrow mesenchymal stem cells. The poor mechanical properties of CS were resolved by combining it with SF. SF has outstanding biodegradability, mechanical strength, and biocompatibility, which can be modified into sponges, gels, films, and nanofibers.[21−23] Moreover, SF promotes cell proliferation over differentiation and thus is useful for various tissue engineering applications including cartilage, bone, liver, and skin.[24,25] The mechanical properties of SF/CS nanofibers could be enhanced through the incorporation of nHAP.[26]

In this work, we introduce the combined approach of SF/CS with osteoconductive nHAP and osteoinductive bone morphogenetic protein-2 (BMP-2). BMP-2 is considered to be the most influential growth factor for bone regeneration.[27] We postulated that, by combining nHAP and BMP-2 in a single nanofibrous scaffold, release of the latter in a controlled manner could result in faster and meticulous bone formation. Previously, the controlled release of BMP-2 from the core of core−shell nanofibers has been studied for bone tissue engineering applications.[28] Because proliferation and osteogenic differentiation of stem cells is sensitive to the dose exposure to BMP-2,[29] a BMP-2 delivery system that could load different BMP-2 concentrations and show different BMP-2 release rates would be desirable. A facile way to explore the enhanced osteoinductive effect from a higher BMP-2 concentration in the culture medium could be achieved by modulating the shell thickness of core−shell nanofibers. Therefore, we aimed to incorporate BMP-2 in the core part of SF/CS/nHAP nanofibers prepared through coaxial electrospinning to promote osteogenesis and to examine the effect of the shell thickness on osteogenesis of human-bone-marrow-derived mesenchymal stem cells (hMSCs). The schematic representation of the preparation of SF/CS/nHAP/BMP-2 nanofibers with thick (SCHB2-thick) and thin (SCHB2-thin) shell morphologies and their influence on hMSCs is hypothetically shown in Scheme 1.

2. EXPERIMENTAL SECTION

2.1. Materials. Chitosan (CS; 98% degree of deacetylation and 1×10^5 Da molecular weight) was purchased from Fluka (Germany), whereas *Bombyx mori* silk was obtained from a farm in Miaoli County, Taiwan. Trifluoroacetic acid (TFA) and dichloromethane (DCM) were procured from J.T. Baker (USA) and Alfa Aesar (U.K.), respectively. Dulbecco's modified Eagle's medium (DMEM) and fetal

DOI: 10.1021/acsami.5b04962
ACS Appl. Mater. Interfaces 2015, 7, 21170−21181

bovine serum (FBS) were purchased from Invitrogen and Gibco, respectively. Recombinant human bone morphogenetic protein-2 (BMP-2) was obtained from Sino Biological Inc. (China). Human-bone-marrow-derived mesenchymal stem cells (hMSCs; HMSC.BM-500) were purchased from Cellular Engineering Technologies Inc. (USA). Fluorescein isothiocyanate labeled bovine serum albumin (FITC-BSA) was obtained from Life Technologies (USA). Except *B. mori* silk, all of the chemicals were used as received without further purification.

2.2. Preparation and Characterization of Nanohydroxyapatite (nHAP) Nanoparticles. nHAP nanoparticles were prepared through a chemical precipitation method, as reported in our previous study and characterized through transmission electron microscopy (TEM), X-ray diffractometry (XRD), and Fourier transform infrared (FTIR) spectrometry.[26]

2.3. Electrospinning of Silk Fibroin (SF)/CS, SF/CS/nHAP, and SF/CS/nHAP/BMP-2 (SCHB2) Nanofibers. SF was prepared from *B. mori* silk by a stepwise purification method.[21] SF/CS and in situ incorporated SF/CS/nHAP (30%) nanofibrous membranes (NFMs) were also prepared as reported earlier.[26] BMP-2-incorporated SCHB2 core−shell nanofibers were prepared in two forms: one with thick (SCHB2-thick) and the other with thin (SCHB2-thin) shell morphology, having BMP-2 in the core. The shell solution was the same as that of SF/CS/nHAP composite nanofibers, and the core solution was 25 μg/mL BMP-2 in phosphate-buffered saline (PBS). The shell thickness was controlled by electrospinning a SCHB2 solution at two different flow rates, viz., a shell flow rate of 0.5 mL/h for SCHB2-thick and 0.3 mL/h for SCHB2-thin, while maintaining the core flow rate at 0.05 mL/h. A coaxial spinneret connected to a dual-pump high-voltage power supply (Jyi Goang Enterprise Ltd., Taiwan) was used to make different core−shell fibers, using two 5 mL syringes. A maximum voltage of 18 kV and a tip−target distance of 12 cm were used to deposit nanofibrous scaffolds on an aluminum target with a membrane thickness within 150−200 μm. The SCHB2-thick and SCHB2-thin NFMs contain 17 and 28 μg of BMP-2/g of NFM, respectively. To remove residual TFA and also to reduce the water solubility of SF, all of the NFMs were immersed in a 7% (v/v) ammonia/75% (v/v) ethanol aqueous solution for 30 min, dried, and stored in a desiccator.[21,26]

2.4. Characterization of NFMs. Surface-coated SCHB2 NFMs were characterized for their morphology by scanning electron microscopy (SEM; Hitachi S3000N) with energy-dispersive X-ray spectroscopy (EDX, Horiba EX-250) for elemental analysis. The average fiber diameter of the SCHB2 NFM was measured by considering at least 100 fibers from 10 different images, using *ImageJ* software. TEM (Hitachi H-7500) was used to record the core−shell morphology of the nanofibers. XRD patterns of NFMs were recorded using a Siemens D5005 X-ray diffractometer (Bruker AXS, Karlsruhe, Germany) with a scanning speed of 2°/min from 5 to 60°. Evaluations on the thermal properties of NFMs were carried out by thermogravimetric analysis (TGA) at 10 °C/min from 25 to 600 °C (TGA 2050, TA Instruments, USA). To characterize the chemical compositions of NFMs, attenuated total reflectance Fourier transform infrared (ATR-FTIR, Horiba Ltd., Kyoto, Japan) spectroscopic investigations were carried out from 400 to 4000 cm^{-1} with 2 cm^{-1} resolution.

2.5. Evaluation on the Release Profile and Bioactivity of BMP-2. The release kinetics of BMP-2 was evaluated by immersing SCHB2 NFMs in PBS for 30 days. Uniformly cut 1.8-cm-diameter NFM disks were immersed in 2 mL of PBS in a 12-well culture plate at 37 °C, and the concentration of BMP-2 in the release medium was determined by a BMP-2 ELISA kit from PeproTech (Rocky Hill, NJ). The cumulative release percentage of BMP-2 with respect to the time was calculated from the original amount of BMP-2 in the NFM. The average values of six samples are reported. To confirm the osteoinductive bioactivity of BMP-2 inside the core−shell fibers, 1.5-cm-diameter SCHB2 NFM disks were immersed in 1.5 mL of a cell culture medium (CCM) (DMEM containing 10% FBS and 1% penicillin−streptomycin) in a 24-well culture plate at 37 °C for 21 days. The CCM containing released BMP-2 was used to culture 5 × 10^3 hMSCs seeded on tissue culture polystyrene (TCPS), and the extent of osteogenic differentiation was determined from alkaline phosphatase (ALP) production by hMSCs under BMP-2 induction. ALP production by the same number of hMSCs seeded on TCPS in fresh CCM was used as the control. The average values of six samples are reported. The effective incorporation of BMP-2 in core−shell fibers was qualitatively examined by a mock study by preparing SF/CS/nHAP/FITC-BSA core−shell nanofibers, and the presence of FITC-BSA in the core of the fiber was examined using a confocal laser scanning microscope (Zeiss LSM 510, Germany).

2.6. In Vitro Experiments. *2.6.1. Cell Proliferation.* hMSCs were seeded on 1.5 cm disk-shaped NFMs in a 24-well plate at a seeding density of 5 × 10^3 cells/cm^2. Cell culture was carried out in 1.5 mL of an osteogenic culture medium (DMEM with 50 μM L-ascorbic acid phosphate, 1% antibiotic-antimycotic, 0.1 μM dexamethasone, 10 mM glycerol 2-phosphate, and 10% FBS) with a medium change every 2−3 days. Quantitative estimation of hMSC proliferation on SF/CS, SF/CS/nHAP, and SCHB2 NFMs was carried out using MTS assay. The optical density (OD) of the solution was measured at 492 nm (OD_{492}) using an ELISA reader (Synergy HT, BioTek, USA).

2.6.2. Cell Viability. Qualitative evaluation of the presence of viable cells in NFMs was accomplished by a Live/Dead Viability/Cytotoxicity kit (Molecular Probes, USA) after culture for 7 and 14 days. All of the samples were incubated with the staining solution at 37 °C for 30 min in a 24-well plate, and the morphology of cells was imaged under a Zeiss LSM 510 Meta confocal laser scanning microscope.

2.6.3. Quantification of the ALP Activity. The intracellular ALP activity of hMSCs was measured using an ALP kit (SensoLyte pNPP ALP assay kit, AnaSpec, USA). The OD was measured at 405 nm using an ELISA reader (OD_{405}). The specific ALP activity per cell basis was reported by normalizing the ALP activity with the cell number from MTS assay and expressed as OD_{405}/OD_{492}.

2.6.4. Mineralization of hMSCs by SEM. After PBS washing, cells were fixed using 4% glutaraldehyde and maintained at room temperature for 2 h, dehydrated, and dried per standard protocols. The morphology of minerals deposited on the sample surface was monitored through SEM (Hitachi S-3000N).

2.6.5. Mineralization of hMSCs by Alizarin Red S (ARS) and von Kossa Staining and Quantification of Calcium Deposition. ARS staining was imparted to estimate the extent of mineral deposition on NFMs by examining the presence of mineralized nodules during hMSC culture. Membranes seeded with hMSCs were fixed with a 2.5% glutaraldehyde solution for 2 h and evaluated for its calcium content at 7, 14, 21, and 28 days of culture. Microphotographs were recorded using an inverted microscope (Olympus IX-71) to estimate the intensity of the red color on membrane surfaces. The amount of calcium deposited on NFMs was quantitatively estimated through cetylpyridinium chloride (CPC) treatment. The concentration of desorbed calcium ions in a CPC solution was read at 540 nm in an ELISA reader (OD_{540}) and normalized to the cell number obtained from the MTS assay (OD_{540}/OD_{492}). The average values of five samples are reported.

For von Kossa staining, cell-seeded samples were fixed with a 2.5% glutaraldehyde solution (dissolved in a 0.1 M phosphate buffer) for 2 h. A silver nitrate/sodium thiosulfate treatment was given first followed by nuclear fast red impregnation as per standard procedures. Photomicrographs of the samples were recorded with an inverted microscope (Olympus IX-71) to estimate the intensity of the brown color on membrane surfaces.

2.6.6. Evaluation of Osteogenic Gene Expression. Expression of various osteogenic differentiation marker genes on NFMs was examined using standard protocols of RNA isolation and cDNA synthesis. Glyceraldehyde 3-phosphate dehydrogenase (housekeeping gene) was used as the internal control for analysis with Bio-Rad software. Real-time quantitative polymerase chain reaction (Q-PCR) measurements were performed using a SYBR Green RT-PCR kit having a Mini Option detection system (Bio-Rad CFD-3120). Collagen type I (COL I), ALP, osteocalcin (OCN), and osteopontin

DOI: 10.1021/acsami.5b04962
ACS Appl. Mater. Interfaces 2015, 7, 21170−21181

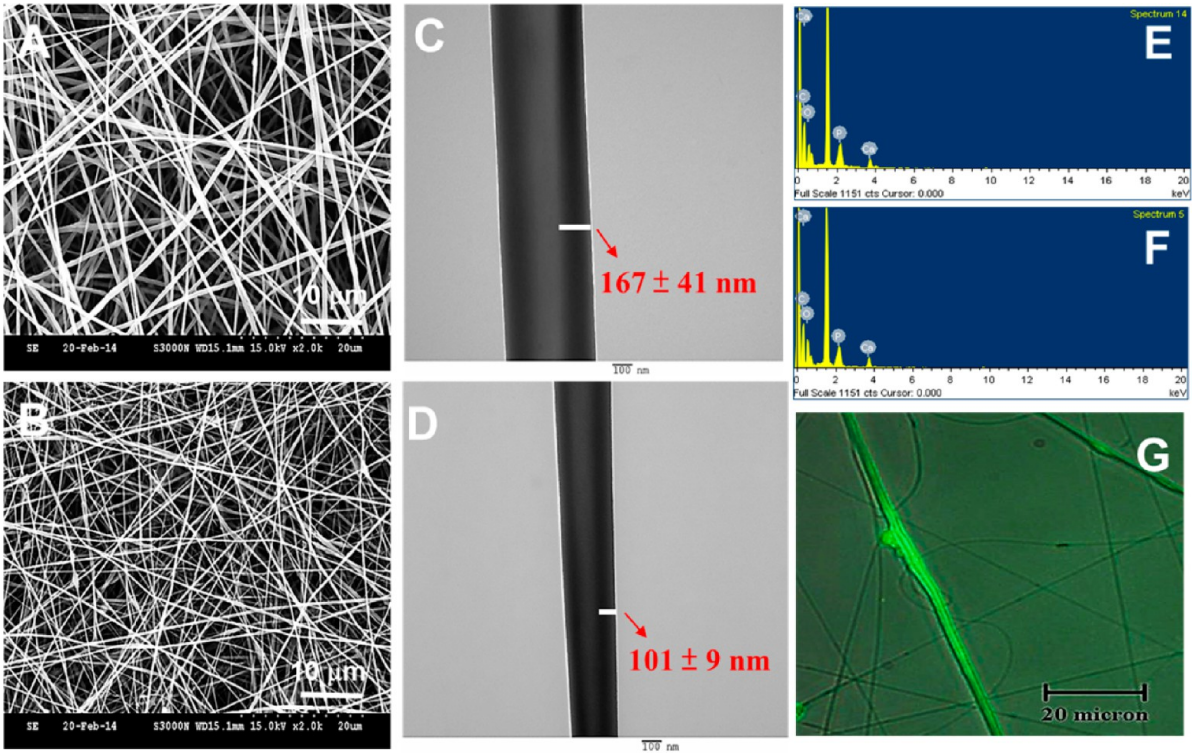

Figure 1. SEM (A and B) and TEM (C and D) images and EDX elemental analysis (E and F) of SCHB2-thick (A, C, and E) and SCHB2-thin (B, D, and F) NFMs. (G) Fluorescent microscopic images of FITC-BSA-incorporated core−shell SCHB2 nanofibers.

(OPN) bone marker genes were selected for analysis using the $2^{-\Delta\Delta ct}$ relative quantification method.[21,26]

2.6.7. Quantification of OCN. The osteogenic differentiation potential of NFMs was examined by determining the concentration of OCN, a biochemical marker for bone formation. The medium was removed after 7 and 21 days of hMSC seeding, and the samples were washed twice with PBS. The amount of OCN was measured using a human osteocalcin instant ELISA kit from eBioscience (San Diego, CA). The average values of five samples are reported.

2.7. In Vivo Study. Animal procedures were performed with the approval from the animal ethical committee of Chang Gung University. Six female nude mice with weights of 20−30 g (6−8 weeks) were used for the studies. SCHB2-thin NFM disks of 1.5 cm diameter seeded with 5×10^4 hMSCs/cm^2 were used as test samples, whereas acellular SCHB2-thin NFMs of the same size were used as controls. The back side of the animals was sterilized with 75% alcohol. Cell-seeded and acellular control samples were implanted subcutaneously, on each side of the back of the animal. After 4 and 8 weeks, animals were sacrificed and implants were harvested for histological and immunohistochemical analysis. The retrieved samples were immersed in 10% formaldehyde, dehydrated, embedded in paraffin wax, and sectioned into 4-μm-thick tissue sections. Samples were deparafinized, treated, and subjected to hematoxylin and eosin (H&E) and Masson's trichrome staining and immunochemistry (IHC) for COL I and OCN. Nonspecific binding sites were blocked by treating the samples with Ultra V Block (Thermo Scientific) for 5 min and incubated in anti-OCN antibody (ab13418) or anti-COL I antibody (ab90395) from Abcam (Cambridge, MA) for 120 min. After successive treatments, samples were counterstained with hematoxylin for 5−10 min, washed, and dried, and the images were recorded under an inverted optical microscope (Olympus IX-71).

2.8. Statistics. All data were expressed as mean ± standard deviation, and the significant differences were determined using a one-way ANOVA LSD test. A value of $p < 0.05$ was considered to be statistically significant.

3. RESULTS AND DISCUSSION

3.1. Characterization of SCHB2 Core−Shell NFMs. HAP particles produced had an average diameter of less than 50 nm and were characterized through various techniques, as reported in our previous work.[26] The weight percentages of BMP-2 in SCHB2 NFMs calculated from the flow rates of core and shell solutions are 17 and 28 μg/g of NFM for SCHB2-thick and SCHB2-thin, respectively. As explained in our previous results,[26] the uses of an ammonia/ethanol solution were to remove possible TFA residuals, to prevent cellular toxicity, and to achieve water insolubility of SF.[30,31]

Core−shell nanofibers exhibited a smooth and beads-free morphology under SEM. From previous results, the observed average fiber diameters of SF/CS and SF/CS/nHAP NFMs were 447 ± 168 and 266 ± 47 nm, respectively.[21,26] However, in coaxial electrospinning, a higher flow rate of the shell solution led to a larger average fiber diameter for the SCHB2-thick NFM (534 ± 147 nm) compared with the SCHB-2-thin NFM (346 ± 47 nm), although the difference in the fiber diameter is not statistically significant (Figure 1A,B). Both SCBH2 NFMs were further investigated for variation in the shell thickness using TEM (Figure 1C,D). The trend observed for the shell thickness correlated with that for the fiber diameter, which is 167 ± 41 nm for the SCHB2-thick NFM and 101 ± 9 nm for the SCHB2-thin NFM.

The SEM/EDX elemental analysis was used to verify the presence of nHAP in SCHB2 NFMs by measuring the stoichiometric ratio of calcium and phosphate. Being the major constituent of bone, HAP could provide an adequate environment for the cells to enhance the osteoconductivity and thus plays a crucial role in the bone formation capability of SF/CS fibers. The molecular stability of nHAP after TFA/DCM exposure could be confirmed from the stoichiometric ratio.[32]

DOI: 10.1021/acsami.5b04962
ACS Appl. Mater. Interfaces 2015, 7, 21170−21181

Parts E and F of Figure 1 show the EDX elemental composition spectra of SCHB2 NFMs, where the atomic percentages of P in SCHB2-thick and SCHB2-thin NFMs are 1.04 and 1.00, respectively. At the same time, the atomic percentages of Ca in SCHB2-thick and SCHB2-thin are 1.77 and 1.65, respectively. Thus, the respective Ca/P ratios of SCHB2-thick and SCHB2-thin NFMs measured through EDX analysis are 1.70 and 1.65. All of the values were matched with the theoretical Ca/P stoichiometric ratio of HAP (1.67) and thus were conclusive for the stability of nHAP in SCHB2 NFMs.

Qualitative measurement on the effectiveness of BMP-2 incorporation in the fiber core was further analyzed through a mock study using FITC-BSA.[33,34] Because BMP-2 has no active fluorochromes to be detected through a fluorescent microscope, FITC-BSA was used to replace BMP-2 to observe the morphology of core−shell fibers that were prepared under the same electrospinning conditions. Figure 1G represents the confocal fluorescent microscopic images of SF/CS/nHAP/FITC-BSA core−shell nanofibers with FITC-BSA in the core and SF/CS/nHAP in the shell. The superior FITC intensity in the core than that in the shell implies the effective incorporation of BMP-2 in the core of SCHB2 core−shell nanofibers. Specifically, the fabrication of core−shell nanofibers using a BMP-2 core solution in PBS could eliminate the exposure of BMP-2 to harmful organic solvents during the electrospinning step and thus facilitate preservation of the osteoinductive activity of this protein.

Further comparison of SCHB2 NFMs with SF/CS and SF/CS/nHAP NFMs by FTIR (Figure S1), XRD (Figure S2), and TGA (Figure S3) confirmed the chemical structure of SCHB2 NFMs.

3.2. Release and Bioactivity of BMP-2. The release rates of BMP-2 from both SCHB2 NFMs were measured from the amount of BMP-2 released at specific time points and the cumulative BMP-2 release percentage.[33] Sustained release of BMP-2 was observed for both SCHB2 NFMs up to 14 days; nonetheless, the concentration of BMP-2 in the release medium is significantly higher for SCHB2-thin than SCHB2-thick NFM during all time points (Figure 2A). From accumulative BMP-2 release percentages (based on the total BMP-2 in each NFM) in Figure 2B, both samples released ~20% BMP-2 at day 1 with SCHB-thin had a higher release rate. This trend, consistently prolonged with the elevated release profile of SCHB-thin, continued up to 14 days and became the plateau for both samples after 80% of BMP-2 was released. The BMP-2 release profiles were analyzed up to 10 days using the Peppas equation:[35]

$$Q = kt^n \quad (1)$$

where Q is the BMP-2 release percentage, t is the release time, k is a constant reflecting the structural and geometric characteristics of the fibers, and n is the release exponent that indicates the release mechanism. The regressed equations are $Q = 19.15t^{0.57}$ (R^2 = 0.9953) and $Q = 25.29t^{0.48}$ (R^2 = 0.9993) for SCB2-thick and SCBH2-thin NFMs, respectively. Thus, the BMP-2 release from both NFMs was via a non-Fickian diffusion mechanism or diffusion coupled with erosion because the values of the release exponent are 0.57 and 0.48 (>0.45). The kinetic constant for SCBH2-thin (25.29) is also higher than that of SCBH2-thick (19.15), as expected. The higher rate of BMP-2 release from the SCBH2-thin NFM could be due to the concerted effect of a higher weight percentage of BMP-2 in the membrane and the reduced shell thickness. Nonetheless,

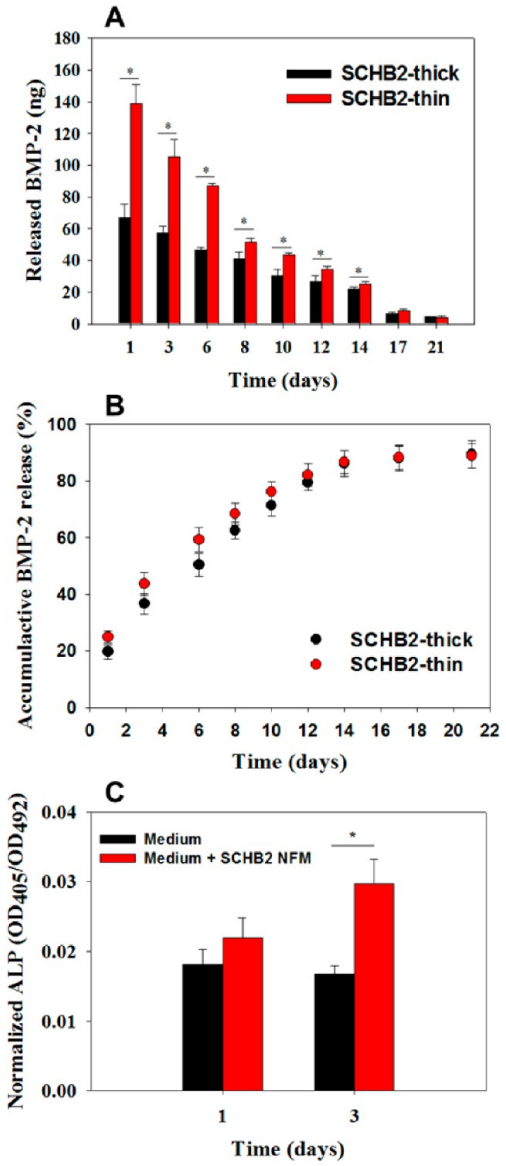

Figure 2. Amount of BMP-2 release at a specific time point (A) and the accumulative BMP-2 release percentage (B) from SCHB2 NFMs. The accumulative percentage is based on the total amount of BMP-2 in each NFM. (C) BMP-2 bioactivity test by measuring the differentiation of hMSCs in the CCM and a BMP-2-released CCM through normalized ALP activity measurements (n = 6). *: $p < 0.05$.

enhanced osteogenic differentiation of hMSCs on the SCHB2-thin NFM is expected from the osteoinductive effect of copious BMP-2 around the cells during cell culture.

Although the release profile is very convincing for the effective incorporation of BMP-2, measurement on the bioactivity is essential to endorse the osteogenic functionality of the NFM for bone tissue engineering. BMP-2 release from the SCHB2 NFM was carried out in a CCM for 21 days. The culture of hMSCs in a BMP-2-released CCM was compared with the CCM up to 3 days to validate the maintenance of the osteoinductive activity of released BMP-2, by measuring the specific ALP production of hMSCs. At day 1, the BMP-2-released CCM shows slightly higher ALP specific activity compared to the CCM, whereas on day 3, a significantly higher amount of ALP was produced by hMSCs (Figure 2C). This elevated ALP specific activity of hMSCs cultured in a BMP-2-

DOI: 10.1021/acsami.5b04962
ACS Appl. Mater. Interfaces 2015, 7, 21170−21181

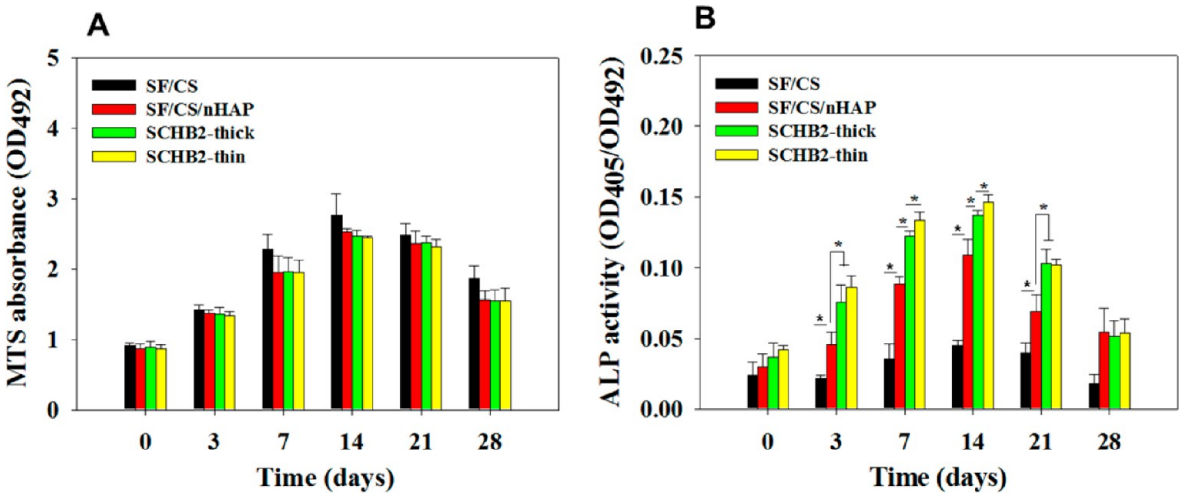

Figure 3. Cell proliferation by MTS assay (A) and normalized ALP activity (B) of hMSCs on different NFMs (n = 5). *: $p < 0.05$.

released CCM confirms that the electrospinning process and ammonia/ethanol postmodification did not destroy the osteoinductive activity of encapsulated BMP-2 in the core and hence endorses the potential of SCHB2 NFMs in bone-specific regeneration.

3.3. In Vitro Experiments. *3.3.1. Cell Proliferation and ALP Activity.* hMSCs were used to evaluate the cytotoxicity of SF/CS, SF/CS/nHAP, and SCHB2 NFMs using MTS assay (Figure 3A). The number of adhered cells on day 0 (4 h) was taken as the reference point for later periods of cell proliferation. Interestingly, the hMSC proliferation rate was almost similar among the NFMs at all times irrespective of the nature of the samples. However, the total number of adhered cells increased with time, up to 14 days, and then decreased on the remaining time points at 21 and 28 days. Our previous studies on SF/CS scaffolds also confirmed the same trend in cell proliferation,[21,26] and we thereby conclude that the incorporation of nHAP and BMP-2 into SF/CS NFMs did not significantly alter the cell attachment and proliferation.

Being an early marker, ALP plays a crucial role in recognizing the initiation of the mineralization process by cell differentiation. Mineralization starts with nucleation of inorganic phosphates and Ca^{2+}, results in calcification, and thereby increases the phosphate concentration in the local environment. This happens by elevation in the mineralization of ECM through the hydrolysis of phosphate esters,[36] in which a downstream cell differentiation factor is promoted by the ALP enzyme to stimulate differentiation of osteoblasts. Therefore, ALP is considered as an early interim osteoblast activity indicator. The normalized ALP activities of hMSCs cultured on different NFMs are shown in Figure 3B. During the culture period from 0 to 28 days, the ALP activity increased from days 0 to 14 and decreased thereafter up to 28 days, and the maximum was at 7 and 14 days. Except on day 0, there is a significant difference in the ALP activity among different samples, irrespective of the culture duration. From days 3 to 21, SCHB2 NFMs had substantially higher ALP activity compared to SF/CS and SF/CS/nHAP NFMs. However, at days 7 and 14, the SCHB2-thin NFM showed significantly higher ALP activity compared to the SCHB2-thick NFM. Because the amount of BMP-2 released from SCHB2-thin was much higher during the initial days of culture (Figure 2A), more BMP-2 was available around the cells, which led to faster osteogenesis of hMSCs and increased production of ALP in the early phase of osteogenic differentiation. Comparable results were observed for ALP production of SF/CS and SF/CS/nHAP NFMs. Similar to the trend shown by SCHB2, SF/CS/nHAP produced a significantly higher amount of ALP compared to SF/CS, throughout the culture period from 3 to 21 days. This phenomenon could be explained on the basis of the osteoconductive nature of nHAP, leading to higher ALP production, as reported in our previous result.[26] The decrease in the specific ALP activity at 21 and 28 days of culture can be correlated with the absence of a ALP expression at the later stages of cell differentiation. These data well-coordinated with the bioactivity and BMP-2 release profile of SCHB2 NFMs in Figure 2.

3.3.2. Live–Dead Staining. The live–dead staining was used to evaluate the cell viability through morphology observation (Figure 4). Although MTS assay for cell viability concludes for no significant difference in the cell number among various membranes at each time point, fibroblast-like spindle cell

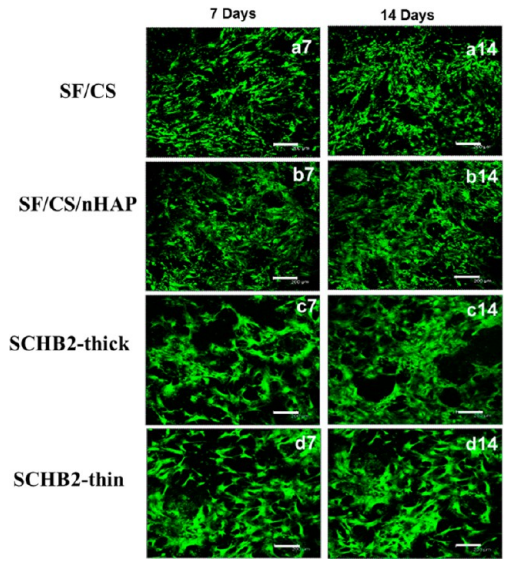

Figure 4. Live–dead staining of hMSCs on SF/CS (a7–a14), SF/CS/nHAP (b7–b14), SCHB2-thick (c7–c14), and SCHB2-thin (d7–d14) NFMs after 7 and 14 days. Bar = 200 μm.

DOI: 10.1021/acsami.5b04962
ACS Appl. Mater. Interfaces 2015, 7, 21170–21181

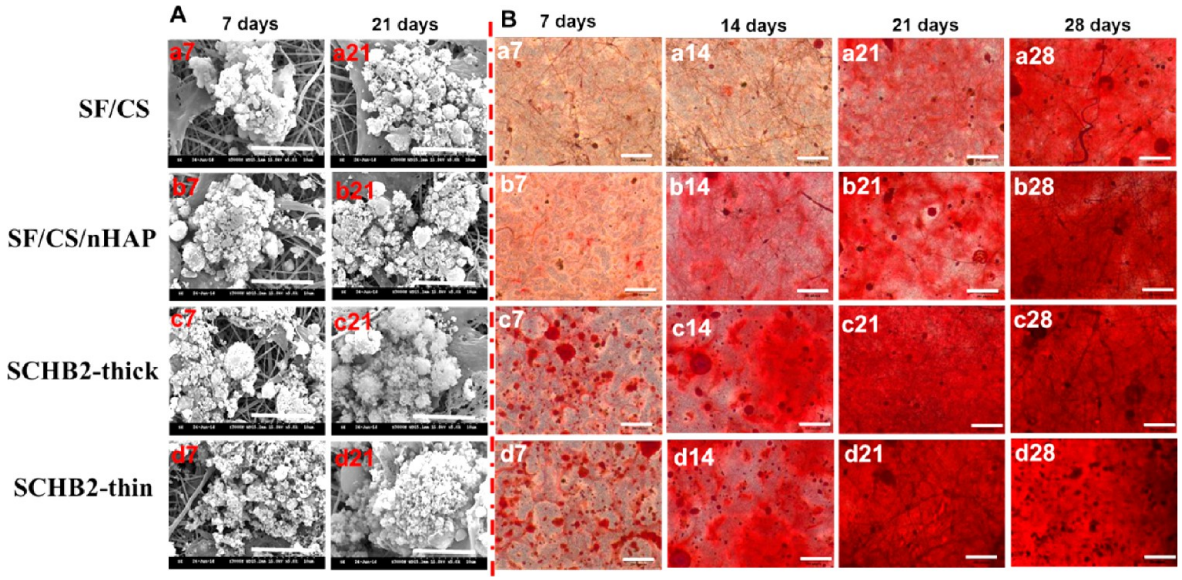

Figure 5. (A) Mineralization of hMSCs on SF/CS, SF/CS/nHAP, SCHB2-thick, and SCHB2-thin NFMs as observed by SEM after 7 and 21 days. Bar = 10 μm. (B) Alizarin red staining of hMSCs on SF/CS, SF/CS/nHAP, SCHB2-thick, and SCHB2-thin NFMs after 7, 14, 21, and 28 days. Bar = 200 μm.

morphology was observed on SF/CS NFMs and SF/CS/nHAP, compared to a cuboidal shape of cells on SCHB2 NFMs, at both time points. According to our previous results, SF and CS in an equilibrium composition would enrich both proliferation and differentiation simultaneously. This is due to the individual effects of both, in which CS supports faster differentiation, whereas SF stimulates proliferation.[21] The presence of osteoconductive component nHAP in the same system has dragged the proliferation−differentiation equilibrium toward the differentiation side. However, the shape of the cells on SF/CS/nHAP was not conclusive to mention the significant effect of nHAP on cell differentiation. In contrast, a well-defined cuboidal morphology is visible for cells on SCHB2 membranes from day 7, indicating the early differentiation of cells toward the osteogenic lineage in the presence of osteoinductive BMP-2. Although hMSCs on SCHB2-thin displayed more differentiation than SCHB2-thick at both times, as shown in the ALP activity results, the shape of the cells from the live−dead staining was not confirmative in defining the enhanced differentiation on the SCHB2-thin NFM. The number of viable cells on day 14 could be correlated with MTS assay in Figure 3A, in which the cell density is only slightly higher than that on day 7. The direct dependence of substrate materials toward cell functionalities like spreading, proliferation, and differentiation is clearly visible here and thus accounts for the enhanced differentiation of SCHB2 NFMs over proliferation. The dependence of substrate characteristics in osteogenic differentiation of hMSCs was reported earlier.[37,38] Thus, the live−dead assay further confirms the effect of osteoinductive components in osteogenic differentiation of hMSCs.

3.3.3. Mineralization by SEM Observation and ARS Staining. The process of secreting inorganic phosphates such as calcium phosphate on substrate surfaces by hMSCs at the middle of the culture period is called mineralization.[39] Various qualitative and quantitative measures such as microscopy, elemental analysis, etc., could be used to examine mineral deposition on the surface of the substrates. SEM images of mineralized cells on NFMs confirmed the relevance of material characteristics and the culture time on hMSC mineralization. Figure 5A represents the SEM images of mineralized hMSCs on SF/CS, SF/CS/nHAP, SCHB2-thick, and SCHB2-thin NFMs at 7 and 21 days. Considering the time dependency, mineralization on all of the substrates was less at day 7, compared to the long-term culture duration of 21 days. This is due to the accumulated deposition of minerals over time. Substrate-dependent mineralization could be verified by observing the density of mineral deposition on various NFMs at both time points. SF/CS shows relatively minimum deposition, while SF/CS/nHAP exhibits higher and SCHB2 the highest deposition. Elevated mineral deposition on SF/CS/nHAP over SF/CS should be due to the presence of osteoconductive nHAP, and at the same time, the presence of both osteoconductive and osteoinductive factors (nHAP and BMP-2) synergistically makes the SCHB2 NFMs potential substrates for bone tissue engineering.

The ARS staining further confirmed the relative potential of NFMs in aiding the deposition of calcium phosphate over the substrate surface. Moreover, ARS staining provides a systematic measure to evaluate the correlation between the duration of culture and the substrate properties. ARS binds with Ca^{2+} through mineralized ECM to make bright-red stains over the sample surface. Optical microscopic images of ARS-stained SF/CS, SF/CS/nHAP, SCHB2-thick, and SCHB2-thin samples at 7, 14, 21, and 28 days are shown in Figure 5B. At day 7, both SF/CS and SF/CS/nHAP displayed slight reddish dots on the substrate surface with domination in intensity for the latter one. However, SCHB2 showed enhanced stain intensity with wider reddish spots. As the culture duration increased to 14 days, SF/CS had a similar staining appearance as 7 day, but SF/CS/nHAP appeared to be significantly denser than the previous time point. Both SCHB2 membranes showed enhanced stain intensity at 14 days but were similar compared to each other. A different trend in enhancing the stain intensity was observed in a 21 day duration, with each sample displaying an increase in the stain intensity on the order of SF/CS with the minimum stain, SF/CS/nHAP with the moderate stain, SCHB2-thick with the higher stain, and SCHB2-thin with the maximum stain.

DOI: 10.1021/acsami.5b04962
ACS Appl. Mater. Interfaces 2015, 7, 21170−21181

This trend was continued to the next time point, 28 days, in which SCHB2 had the maximum and SF/CS had the minimum staining intensity among the four samples. The ARS staining on both SCHB2 membranes appeared to be saturated with no distinguishable difference in the stain intensity. However, the maximum stain intensity of SCHB2-thin at day 21 can be attributed to the presence of a higher amount of osteoinductive BMP-2 in the CCM (Figure 2A) along with osteoconductive nHAP in the fiber shell. This indicates the relative potential of SCHB2-thin NFMs in hMSC differentiation toward the osteogenic lineage.

3.3.4. Mineralization by Calcium Quantification and von Kossa Staining. Besides microscopic observations, 10% CPC treatment that can extract ARS bound to Ca^{2+} on the cell surface was given to each membrane for the quantitative evaluation of hMSC mineralization (Figure 6). As observed in the ARS staining results, the normalized calcium content increased with time from days 7 to 28. At days 7, 14, and 21, both SCHB2 membranes showed significantly higher calcium content compared to SF/CS and SF/CS/nHAP. Moreover, the calcium content is significantly higher for SCHB2-thin than SCHB2-thick at days 14 and 21. Interestingly, all samples had only a remarkable difference on day 21, as observed at the same time point in ARS staining (Figure 5B). Although the calcium quantification value was higher at day 28, there was no significant difference among the various samples with nHAP. This could be ascribed to the saturation of ARS on the substrate surface, making it impossible to differentiate the exact amount of bound ARS (or deposited calcium).

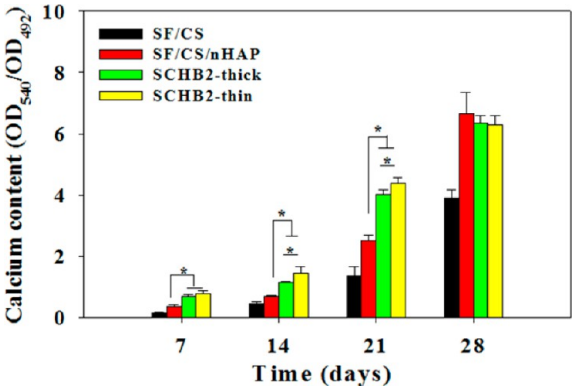

Figure 6. Calcium content of hMSCs cultured on SF/CS, SF/CS/nHAP, SCHB2-thick, and SCHB2-thin NFMs (n = 5). *: $p < 0.05$.

Similar to ARS, von Kossa staining also was used to confirm mineralization of hMSCs on the substrate surface. Because the ability to deposit minerals is a marker of hMSC differentiation, von Kossa could be successfully implemented to assess the differentiation potential of a scaffold in bone tissue engineering. Figure 7 contains the von Kossa staining images on SF/CS, SF/CS/nHAP, SCHB2-thick, and SCHB2-thin NFMs after 14 and 28 days. As observed in ARS staining, von Kossa staining also exhibited a time- and substrate-dependent mineralization of hMSCs. It produces dark brown to black stains on mineralized nodules, and the intensity of the stain is directly proportional to the extent of mineralization. At day 14, all of the samples showed adequate staining, with SCHB2 having the maximum mineralized nodules. SF/CS had minimum staining compared to NFM with nHAP. However, the presence of BMP-2 enhanced the staining because differentiation was higher on the SCHB2 samples. SF/CS displayed negligible differences in the stain intensity while considering the 28 day sample, but SF/CS/nHAP had a slightly darker stained appearance compared to the former. As expected, both SCHB2 NFMs had the maximum staining intensity at day 28, confirming the effect of BMP-2 in osteogenic differentiation. Qualitative assessment to distinguish the staining density difference between SCHB2 NFMs was quite difficult, although the rest of the experimental results could be put forward to choose the ideal NFM for further analysis.

3.3.5. Gene Expression and OCN Quantification. Three major stages of transformations, namely, proliferation, maturation, and mineralization of ECM, exist in the growth and differentiation of hMSCs to the osteoblast lineage, with up-regulation of certain genes followed by down-regulation of other genes.[40] Conferring to the different stages of transformations, various markers are expressed at early, middle, and later stages of cell cycles. The expression of various osteogenic differentiation marker genes, including COL I, ALP, OCN, and

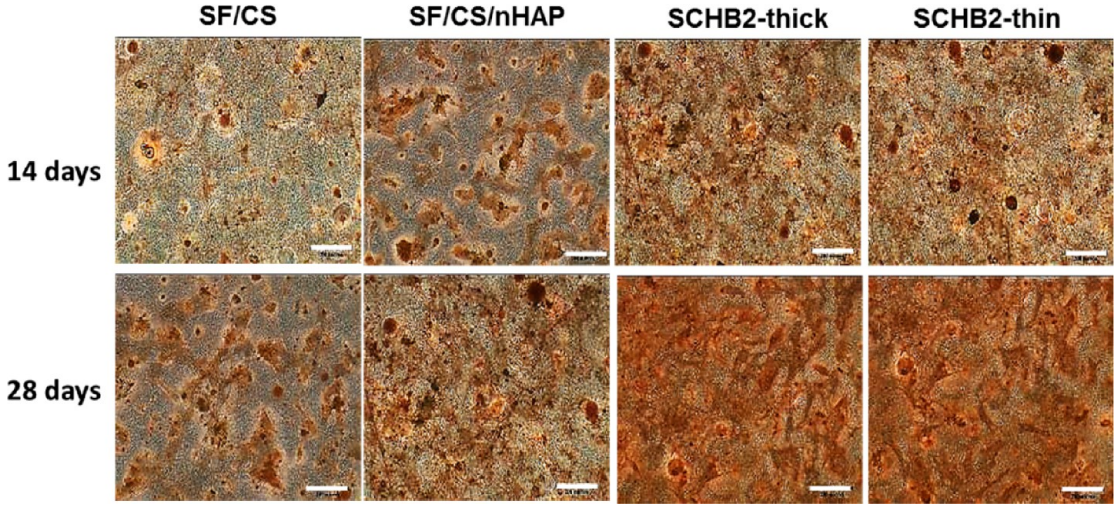

Figure 7. von Kossa staining of mineral deposition of hMSCs cultured on SF/CS, SF/CS/nHAP, SCHB2-thick, and SCHB2-thin NFMs for 14 and 28 days. Bar = 200 μm.

DOI: 10.1021/acsami.5b04962
ACS Appl. Mater. Interfaces 2015, 7, 21170−21181

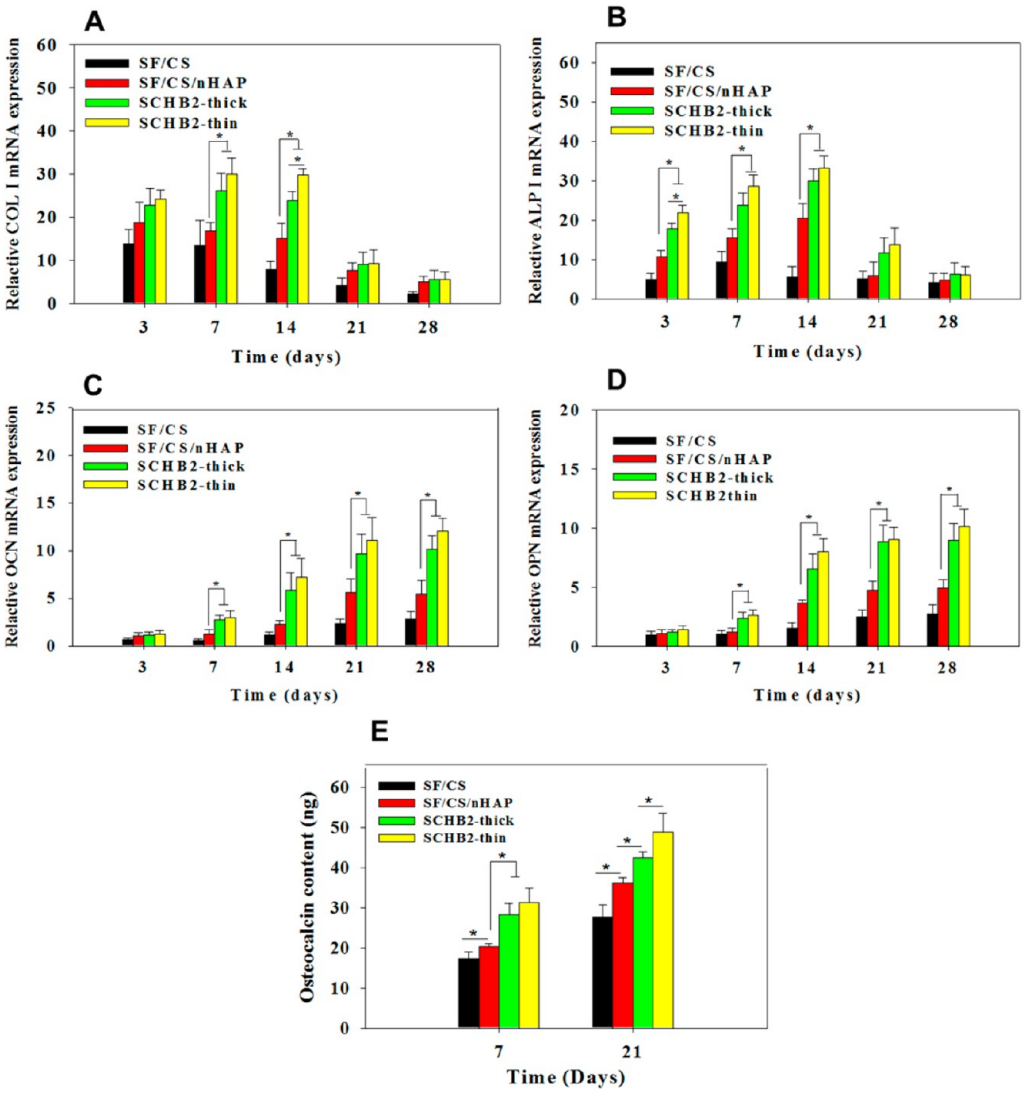

Figure 8. Expression of COL I (A), ALP (B), OCN (C), and OPN (D) osteogenic marker genes and (E) OCN quantification of hMSCs cultured on SF/CS, SF/CS/nHAP, SCHB2-thick, and SCHB2-thin NFMs (n = 5). *: $p < 0.05$.

OPN, are compared in Figure 8A–D as relative mRNA expressions with a culture period duration from 3 to 28 days. COL I and ALP belong to the early differentiation stage, while OPN and OCN are expressed at the middle-to-later stages of hMSC differentiation. Because the expression of ALP and COL I genes is at the early stages of cell differentiation, the relative mRNA expressions of the same was up-regulated at the first 2 weeks of hMSC differentiation. At day 3, all of the NFMs exhibited a moderate level of ALP and COL I expression, enhanced further on day 7 and reaching the maximum on day 14. A down-regulated expression was found thereafter, on days 21 and 28. Both expressions could be correlated with the trend shown in the ALP activity (Figure 3B). The late expression of OCN and OPN was confirmed by observing the maximum expression on day 28 compared to the lower value at early stages.

Apart from the culture duration, substrate-dependent analysis on gene expression endorses the effect of osteoconductive or osteoinductive materials in controlling the up–down-regulations of various osteogenic markers. In this case, being early markers, COL I and ALP show similar trends of substrate characteristics toward gene expression, in which SF/CS shows the minimum and the SCHB2-thin NFM shows the maximum expression throughout the culture period. The ALP expression of SCHB2 was potentially higher on all three early time points (3, 7, and 14 days), while COL I displayed significantly higher values for SCHB2 on days 7 and 14 only. However, SCHB2-thin displayed significantly higher expressions of COL I and ALP on days 3 and 14, respectively, confirming the superior effect of the core–shell fibers with thin shell morphology toward osteogenic differentiation. This could be ascribed to the enhanced osteoinductive effect of the higher BMP-2 concentration in the culture medium for SCHB2-thin up to 14 days (Figure 2A). It further explains the combinational effect of osteoconductive and osteoinductive factors toward hMSC differentiation. A different scenario in substrate-dependent gene expression was observed for the late markers OCN and OPN. Contradictory to ALP and COL I, OCN and OPN showed a linear increase in the relative expression during the culture period from days 3 to 28. Except on day 3, the SCHB2 NFM revealed its potential in inducing hMSCs to express significantly higher levels of mRNA compared to SF/CS and SF/CS/nHAP NFMs. The up–down-regulations of genes denote the cell cycle behavior with respect to the substrate

DOI: 10.1021/acsami.5b04962
ACS Appl. Mater. Interfaces 2015, 7, 21170–21181

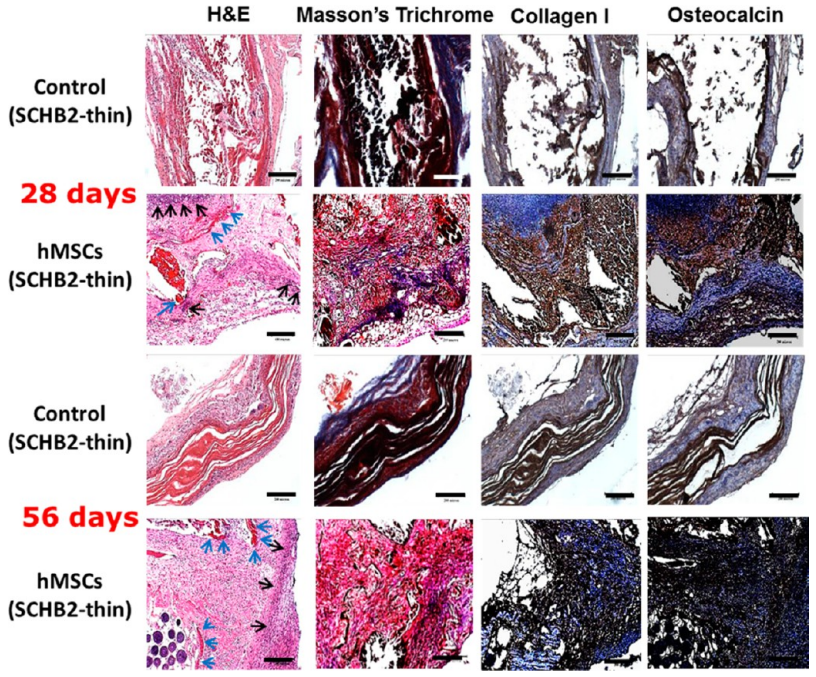

Figure 9. Histological staining (H&E and Masson's trichrome) and immunohistochemical staining of COL I and OCN of acellular control and hMSC-seeded SCHB2-thin NFMs after 4 and 8 weeks of subcutaneous implantation in nude mice. Black arrows denote osteoblasts in the bone matrix, while blue arrows denote osteoids. Bar = 200 μm.

properties and time and hence suggest that the BMP-2 concentration released from the NFM plays a crucial role in cell differentiation toward the osteogenic lineage. Because of the presence of nHAP and BMP-2, mineralization of hMSCs must be substantially higher on SCHB2 membranes and that could be the reason behind the elevated values of OCN/OPN expression at these stages. With a comparison of the SCHB2 membranes, an increase in the OCN and OPN mRNA levels was noted in SCHB2-thin compared to SCHB2-thick, but this increase was not significant.

To further verify gene expression, protein concentration analysis was performed to estimate the quantity of OCN produced at days 7 and 21, during hMSC culture (Figure 8E). In comparison with gene expression, OCN production at day 21 clarifies the relevance of SCHB2-thin compared to all other samples in terms of the osteogenic differentiation potential. At day 7, SF/CS/nHAP showed a significantly higher amount of OCN compared to SF/CS and a lower level compared to SCHB2, as observed in gene expression of OCN. However, the OCN level at day 21 portrays a more specific and accurate picture for the potential of SCHB2-thin toward differentiation because it has significantly higher OCN production. Considering gene expression and the OCN quantification results, the SCHB2-thin NFM can be suggested as an ideal candidate for bone regeneration and thus could be introduced as a potential scaffold for in vivo studies.

3.4. In Vivo Studies. SCHB2-thin NFMs were selected for implantation based on the bone regeneration capability observed from in vitro results. Membranes were seeded with hMSCs, allowed to differentiate for 14 days, and implanted on the back side of nude mice. After 4 and 8 weeks, all of the animals were anesthetized, sacrificed, and evaluated for bone formation. As discussed in our previous results, SF/CS/nHAP NFMs were found to be excellent in bone regeneration, with the presence of osteoconductive nHAP in the membrane.[26] However, in this work, we further examined the possibilities of introducing an additional inducing factor BMP-2, along with nHAP, to enhance osteogenesis of hMSCs, if any. Figure S4A is a photograph of the cell-seeded SCHB2-thin NFM prior to implantation, and Figure S4B shows the harvested membrane from nude mice 8 weeks after implantation.

The retrieved specimen was evaluated by histology and IHC (Figure 9). Induction for bone formation and tissue development was confirmed in comparison with acellular controls, through various histological analysis including H&E, Masson's trichrome, and IHC for COL I and OCN. H&E staining endorses a drastic change in the cell number in comparison with acellular control samples. The dark-violet background for both the 4 and 8 weeks samples represents the existence of osteoblasts (black arrows) in the bone matrix, while the purple color denotes osteoids (blue arrows). At both 4 and 8 weeks, the acellular control NFM was more visible as a reddish-violet color because of cell ingrowth into the scaffold premises from surrounding tissues. For longer periods such as 8 weeks, the intensity of the reddish-violet color decreased and the cell density increased because of in vivo degradation. This observation was consistent in all types of staining, showing the possibility of outside tissue ingrowth over an acellular control membrane. Further verifications on differetiation were performed through Masson's trichrome staining, through which are revealsed osteoids as blue stains in sections of cell-seeded NFMs. When hMSCs differentiated into osteoblasts, osteoids were embedded in the newly formed tissue matrix. This can be observed at the middle part of the 4-week and the right middle part of the 8-week cell-seeded samples.

The confirmative evidence of bone regeneration was further established through IHC for COL I and OCN. Irrespective of the duration, both IHC results display intense brown stains for cell-seeded samples compared to acellular controls. However, the stain intensity was maximum at 8 weeks for both samples,

DOI: 10.1021/acsami.5b04962
ACS Appl. Mater. Interfaces 2015, 7, 21170−21181

confirming continued proliferation and osteogenic differentiation of hMSCs in vivo. The staining intensity was much higher for OCN than COL I at 8 weeks for cell-seeded samples, indicating the relevance of the late expression of OCN in leu of the early expression of COL I. Moreover, the presence of a purple color in cell-seeded samples can be attributed to the presence of a cell nucleus, which is not very intense in control samples. Thus, the results specify the efficacy of cell-seeded SCHB2-thin NFMs toward bone formation, which is conferred through the synergistic effect of osteoconductive nHAP and osteoinductive BMP-2 in a single system. Taken together, the SCHB2-thin NFM is a potential candidate for a bone repair and regeneration process in vivo.

4. CONCLUSION

Core−shell nanofibers with osteoconductive SF/CS/nHAP shells of different thicknesses and osteoinductive BMP-2 cores (SCHB2) were prepared through coaxial electrospinning and compared with SF/CS/nHAP and SF/CS nanofibers. The microscopic characterization revealed the thin and thick shell morphology, while spectroscopic and thermal evaluations confirmed the presence of both nHAP and BMP-2 in SCHB2 NFMs. BMP-2 release kinetics confirmed the accumulated release up to 80% within 2 weeks with SCHB2-thin releasing more BMP-2. Retention of the osteoinductive activity of released BMP-2 could be confirmed through hMSC osteogenic differentiation by released BMP-2 in the medium. The cytocompatibility of the SCHB2 membranes was verified through MTS assay, while osteogenic differentiation of hMSCs was proven from ALP activity assay. The live−dead assay confirmed the number and morphology changes of live cells present in the NFMs at various time periods of cell culture. The osteogenesis potentials of inducing factors toward hMSC mineralization on NFMs could be confirmed through ARS and von Kossa staining. A cross-confirmation of mineralization was quantitatively verified by measuring the calcium content. Gene expression studies by Q-PCR evidenced the presence of early (ALP), middle (COL I and OPN), and late (OCN) bone marker genes at various stages of cell culture from days 0 to 28. In addition, the quantification of OCN highlighted the enhanced osteogenesis potential of SCHB2-thin among all NFMs. The in vivo implantation of hMSCs/SCHB2-thin NFMs constructs confirmed the ectopic bone regeneration capability of SCHB2-thin NFMs as analyzed through IHC for COL I and OCN and histological characterization. Taken together, SCHB2-thin NFMs could be suggested as a promising material for bone-specific tissue regeneration.

■ ASSOCIATED CONTENT

Supporting Information

The Supporting Information is available free of charge on the ACS Publications website at DOI: 10.1021/acsami.5b04962.

Experimental details and FTIR spectroscopy, XRD, TGA, and a gross view from in vivo study (Figures S1−S4) (PDF)

■ AUTHOR INFORMATION

Corresponding Author

*Tel: +886-3-2118800. Fax: +886-3-2118668. E-mail: jpchen@mail.cgu.edu.tw.

Author Contributions

‡K.T.S. and G.-J.L. contributed equally to this work.

Notes

The authors declare no competing financial interest.

■ ACKNOWLEDGMENTS

We are thankful for financial support from the National Science Council, Taiwan, Republic of China (Grants NSC-100-2221-E-182-024 and NSC-101-2221-E-182-029) and Chang Gung Memorial Hospital (Grants CRRPD5C0201-3 and CMRPD3D0201-2).

■ REFERENCES

(1) Langer, R.; Vacanti, J. P. Tissue Engineering. *Science* **1993**, *260*, 920−926.

(2) Wu, S.; Liu, X.; Yeung, K. W. K.; Liu, C.; Yang, X. Biomimetic Porous Scaffolds for Bone Tissue Engineering. *Mater. Sci. Eng., R* **2014**, *80*, 1−36.

(3) Parsons, A. J.; Ahmed, I.; Han, N.; Felfel, R.; Rudd, C. D. Mimicking Bone Structure and Function with Structural Composite Materials. *J. Bionic Eng.* **2010**, *7*, S1−S10.

(4) Liu, Y.; Lim, J.; Teoh, S.-H. Review: Development of Clinically Relevant Scaffolds for Vascularised Bone Tissue Engineering. *Biotechnol. Adv.* **2013**, *31*, 688−705.

(5) Venkatesan, J.; Bhatnagar, I.; Manivasagan, P.; Kang, K. H.; Kim, S. K. Alginate Composites for Bone Tissue Engineering: A Review. *Int. J. Biol. Macromol.* **2015**, *72*, 269−281.

(6) Liu, X.; Ma, P. X. Polymeric Scaffolds for Bone Tissue Engineering. *Ann. Biomed. Eng.* **2004**, *32*, 477−486.

(7) Khandaker, M.; Vaughan, M. B.; Morris, T. L.; White, J. J.; Meng, Z. Effect of Additive Particles on Mechanical, Thermal, and Cell Functioning Properties of Poly(Methyl Methacrylate) Cement. *Int. J. Nanomed.* **2014**, *9*, 2699−2712.

(8) Samorezov, J. E.; Alsberg, E. Spatial Regulation of Controlled Bioactive Factor Delivery for Bone Tissue Engineering. *Adv. Drug Delivery Rev.* **2015**, *84*, 45−67.

(9) Coelho, P. G.; Hollister, S. J.; Flanagan, C. L.; Fernandes, P. R. Bioresorbable Scaffolds for Bone Tissue Engineering: Optimal Design, Fabrication, Mechanical Testing and Scale-Size Effects Analysis. *Med. Eng. Phys.* **2015**, *37*, 287−296.

(10) Rezwan, K.; Chen, Q. Z.; Blaker, J. J.; Boccaccini, A. R. Biodegradable and Bioactive Porous Polymer/Inorganic Composite Scaffolds for Bone Tissue Engineering. *Biomaterials* **2006**, *27*, 3413−3431.

(11) Chen, J. P.; Tsai, M. J.; Liao, H. T. Incorporation of Biphasic Calcium Phosphate Microparticles in Injectable Thermoresponsive Hydrogel Modulates Bone Cell Proliferation and Differentiation. *Colloids Surf., B* **2013**, *110*, 120−129.

(12) Liao, H. T.; Chen, C. T.; Chen, C. H.; Chen, J. P.; Tsai, J. C. Combination of Guided Osteogenesis with Autologous Platelet-Rich Fibrin Glue and Mesenchymal Stem Cell for Mandibular Reconstruction. *J. Trauma* **2011**, *70*, 228−237.

(13) Sumitha, M. S.; Shalumon, K. T.; Sreeja, V. N.; Jayakumar, R.; Nair, S. V.; Menon, D. Biocompatible and Antibacterial Nanofibrous Poly(ϵ-caprolactone)-Nanosilver Composite Scaffolds for Tissue Engineering Applications. *J. Macromol. Sci., Part A: Pure Appl.Chem.* **2012**, *49*, 131−138.

(14) Kim, H.; Park, I.; Kim, J.; Cho, C.; Kim, M. Gas Foaming Fabrication of Porous Biphasic Calcium Phosphate for Bone Regeneration. *Tissue Eng. Regener. Med.* **2012**, *9*, 63−68.

(15) Offeddu, G. S.; Ashworth, J. C.; Cameron, R. E.; Oyen, M. L. Multi-Scale Mechanical Response of Freeze-Dried Collagen Scaffolds for Tissue Engineering Applications. J. Mech. Behav. *Biomed. Mater.* **2015**, *42*, 19−25.

(16) Sadiasa, A.; Nguyen, T. H.; Lee, B. T. In Vitro and in Vivo Evaluation of Porous PCL-PLLA 3D Polymer Scaffolds Fabricated Via Salt Leaching Method for Bone Tissue Engineering Applications. *J. Biomater. Sci., Polym. Ed.* **2014**, *25*, 150−167.

(17) Bhardwaj, N.; Nguyen, Q. T.; Chen, A. C.; Kaplan, D. L.; Sah, R. L.; Kundu, S. C. Potential Of 3-D Tissue Constructs Engineered from

DOI: 10.1021/acsami.5b04962
ACS Appl. Mater. Interfaces 2015, 7, 21170−21181

Bovine Chondrocytes/Silk Fibroin-Chitosan for in Vitro Cartilage Tissue Engineering. *Biomaterials* **2011**, *32*, 5773−5781.
(18) Thavornyutikarn, B.; Chantarapanich, N.; Sitthiseripratip, K.; Thouas, G.; Chen, Q. Bone Tissue Engineering Scaffolding: Computer-Aided Scaffolding Techniques. *Prog. Biomater.* **2014**, *3*, 61−102.
(19) Huang, Z.-M.; Zhang, Y. Z.; Kotaki, M.; Ramakrishna, S. A Review on Polymer Nanofibers by Electrospinning and Their Applications in Nanocomposites. Compos. *Compos. Sci. Technol.* **2003**, *63*, 2223−2253.
(20) Chang, K. H.; Liao, H. T.; Chen, J. P. Preparation and Characterization of Gelatin/Hyaluronic Acid Cryogels for Adipose Tissue Engineering: In Vitro and in Vivo Studies. *Acta Biomater.* **2013**, *9*, 9012−9026.
(21) Lai, G. J.; Shalumon, K. T.; Chen, S. H.; Chen, J. P. Composite Chitosan/Silk Fibroin Nanofibers for Modulation of Osteogenic Differentiation and Proliferation of Human Mesenchymal Stem Cells. *Carbohydr. Polym.* **2014**, *111*, 288−297.
(22) Li, C.; Vepari, C.; Jin, H. J.; Kim, H. J.; Kaplan, D. L. Electrospun Silk-BMP-2 Scaffolds for Bone Tissue Engineering. *Biomaterials* **2006**, *27*, 3115−3124.
(23) Vepari, C.; Kaplan, D. L. Silk as A Biomaterial. *Prog. Polym. Sci.* **2007**, *32*, 991−1007.
(24) Hu, K.; Lv, Q.; Cui, F. Z.; Feng, Q. L.; Kong, X. D.; Wang, H. L.; Huang, L. Y.; Li, T. Biocompatible Fibroin Blended Films with Recombinant Human-Like Collagen for Hepatic Tissue Engineering. *J. Bioact. Compat. Polym.* **2006**, *21*, 23−37.
(25) Wang, Y.; Kim, H. J.; Vunjak-Novakovic, G.; Kaplan, D. L. Stem Cell-Based Tissue Engineering with Silk Biomaterials. *Biomaterials* **2006**, *27*, 6064−6082.
(26) Chen, J. P.; Lai, G. J.; Shalumon, K. T. Response of Human Mesenchymal Stem Cells to Intrafibrillar Nanohydroxyapatite Content and Extrafibrillar Nanohydroxyapatite in Biomimetic Chitosan/Silk Fibroin/Nanohydroxyapatite Nanofibrous Membrane Scaffolds. *Int. J. Nanomed.* **2015**, *10*, 567−584.
(27) Hari Reddi, A. Regulation of Cartilage and Bone Differentiation by Bone Morphogenetic Proteins. *Curr. Opin. Cell Biol.* **1992**, *4*, 850−855.
(28) Zhu, H.; Yu, D.; Zhou, Y.; Wang, C.; Gao, M.; Jiang, H.; Wang, H. Biological Activity of A Nanofibrous Barrier Membrane Containing Bone Morphogenetic Protein Formed by Core-Shell Electrospinning as A Sustained Delivery Vehicle. *J. Biomed. Mater. Res., Part B* **2013**, *101B*, 541−552.
(29) Schofer, M. D.; Fuchs-Winkelmann, S.; Grabedunkel, C.; Wack, C.; Dersch, R.; Rudisile, M.; Wendorff, J. H.; Greiner, A.; Paletta, J. R.; Boudriot, U. Influence of Poly(L-Lactic Acid) Nanofibers and BMP-2-Containing Poly(L-Lactic Acid) Nanofibers on Growth and Osteogenic Differentiation of Human Mesenchymal Stem Cells. *Sci. World J.* **2008**, *8*, 1269−1279.
(30) Hasegawa, M.; Isogai, A.; Onabe, F.; Usuda, M. Dissolving States of Cellulose and Chitosan in Trifluoroacetic Acid. *J. Appl. Polym. Sci.* **1992**, *45*, 1857−1863.
(31) Matsuda, A.; Kagata, G.; Kino, R.; Tanaka, J. Preparation of Chitosan Nanofiber Tube by Electrospinning. *J. Nanosci. Nanotechnol.* **2007**, *7*, 852−855.
(32) Chen, J. P.; Chang, Y. S. Preparation and Characterization of Composite Nanofibers of Polycaprolactone and Nanohydroxyapatite for Osteogenic Differentiation of Mesenchymal Stem Cells. *Colloids Surf., B* **2011**, *86*, 169−175.
(33) Su, Y.; Su, Q.; Liu, W.; Lim, M.; Venugopal, J. R.; Mo, X.; Ramakrishna, S.; Al-Deyab, S. S.; El-Newehy, M. Controlled Release of Bone Morphogenetic Protein 2 and Dexamethasone Loaded In Core−Shell PLLACL−Collagen Fibers for Use In Bone Tissue Engineering. *Acta Biomater.* **2012**, *8*, 763−771.
(34) Yan, S.; Xiaoqiang, L.; Lianjiang, T.; Chen, H.; Xiumei, M. Poly(L-Lactide-co-ε-Caprolactone) Electrospun Nanofibers for Encapsulating and Sustained Releasing Proteins. *Polymer* **2009**, *50*, 4212−4219.
(35) Peppas, N. A. Analysis of Fickian and Non-Fickian Drug Release from Polymers. *Pharm. Acta Helv.* **1985**, *60*, 110−111.
(36) Ogata, K.; Imazato, S.; Ehara, A.; Ebisu, S.; Kinomoto, Y.; Nakano, T.; Umakoshi, Y. Comparison of Osteoblast Responses to Hydroxyapatite and Hydroxyapatite/Soluble Calcium Phosphate Composites. *J. Biomed. Mater. Res., Part A* **2005**, *72A*, 127−135.
(37) Lee, J. H.; Rim, N. G.; Jung, H. S.; Shin, H. Control of Osteogenic Differentiation and Mineralization of Human Mesenchymal Stem Cells on Composite Nanofibers Containing Poly[Lactic-co-(Glycolic Acid)] and Hydroxyapatite. *Macromol. Biosci.* **2010**, *10*, 173−182.
(38) Ko, E. K.; Jeong, S. I.; Rim, N. G.; Lee, Y. M.; Shin, H.; Lee, B. K. In Vitro Osteogenic Differentiation of Human Mesenchymal Stem Cells and In Vivo Bone Formation in Composite Nanofiber Meshes. *Tissue Eng., Part A* **2008**, *14*, 2105−2119.
(39) Toskas, G.; Cherif, C.; Hund, R.-D.; Laourine, E.; Mahltig, B.; Fahmi, A.; Heinemann, C.; Hanke, T. Chitosan(PEO)/Silica Hybrid Nanofibers as a Potential Biomaterial for Bone Regeneration. *Carbohydr. Polym.* **2013**, *94*, 713−722.
(40) Setzer, B.; Bächle, M.; Metzger, M. C.; Kohal, R. J. The Gene-Expression and Phenotypic Response of hFOB 1.19 Osteoblasts to Surface-Modified Titanium and Zirconia. *Biomaterials* **2009**, *30*, 979−990.

DOI: 10.1021/acsami.5b04962
ACS Appl. Mater. Interfaces 2015, 7, 21170−21181